A Brief Description of the South Atlantic Subtropical Gyre: geostrophic circulation patterns and Sverdrup theory validation

Tiago Carrilho Biló
C# 11950866
tcb46@miami.edu

Rosenstiel School of Marine and Atmospheric Science - Large-Scale Ocean Circulation (MPO 712) - Project Report

April 20, 2016

1 Introduction

As part of the **Large-Scale Ocean Circulation (MPO 712)** coursework project, the goal of the present report is to briefly describe the depth-dependent and vertically integrated geostrophic circulation patterns of the South Atlantic Subtropical Gyre between ∼5°S-50°S (see Figure 1). I tried to built a connection between the different large-scale circulation theories learned in class and the real ocean by "answering" the following proposed questions:

1. How does the geostrophic circulation change with depth?
2. To what depth does the gyre circulation extend, and how does this vary with location within the gyre?
3. To what degree is the circulation consistent with Sverdrup theory, and how do the results compare to what is known about the transport of the respective western boundary currents?
4. Are there any interesting features that may be associated with non-Sverdrupian dynamics, and what are they related to?

2 Data and Methods

2.1 Datasets

I explored two distinct and independent datasets. The first dataset is the 1°x1° climatology (http://-apdrc.soest.hawaii.edu) of the absolute Mean Dynamic Topography $[D(x,y,z,t)]$ distributions derived from the combination of ARGO floats in situ measurements (i. e., temperature and salinity profiles), satellite-based geoid models from the Gravity Recovery and Climate Experiment (GRACE), and satellite altimetric data (*Rio et al.*, 2011).

The second dataset corresponds to the 1/8°x1/8° wind stress curl $[\nabla \times \tau(x,y,t)]$ distributions from the Scatterometer Climatology of Ocean Winds (SCOW, data access at http://cioss.coas.oregonstate.edu/scow/). The sea surface wind are computed from the QuikSCAT Scatterometer data (*Risien and Chelton*, 2008). Both datasets are global, however we explore the Subtropical South Atlantic subset indicated by the area inside the black square of Figure 1.

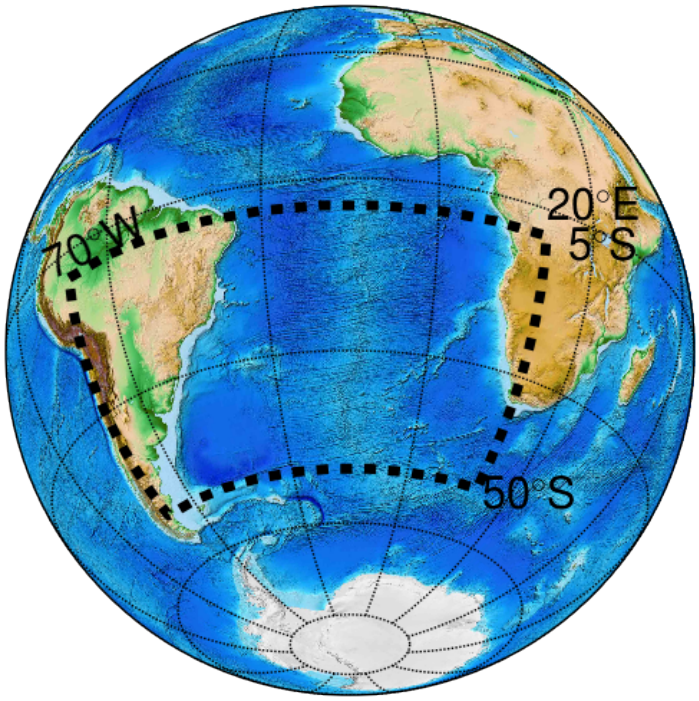

Figure 1: Map of the study area. The black dashed square represents the portion of the South Atlantic where I focused my analysis in order to answer the questions about the subtropical circulation.

2.2 Methods

For simplicity, I conducted the data description and discussion based on the stream function (ψ) distributions. Basically, I applied 3 methodologies/theories in this project: (i) Dynamic Method, (ii) Sverdrup theory, and (iii) Ekman theory. I used the methodology (i) to compute the meridional component of the geostrophic velocities [$V(x,y,z,t)_{geos.}$] from D (Equation 1).

$$V_{geos.} = \frac{10}{f}\frac{\partial D}{\partial x}, \tag{1}$$

(e. g., *Talley et al.*, 2011)

where f is the Coriolis parameter and x is the zonal axis (i. e., latitudinal circles). The theories (ii) and (iii) allowed me to compute the **vertically integrated wind-driven** geostrophic meridional volume transport (M^y at Equation 2).

$$\begin{cases} \text{Sverdrup: } M^y_{sv.} = \frac{\nabla\times\tau}{\rho_0\beta}, \\ \text{Ekman: } M^y_{ek.} = -\frac{\tau^x}{\rho_0 f}, \\ \text{Geostrophic: } M^y_{geos.} = M^y_{sv.} - M^y_{ek.}, \end{cases} \tag{2}$$

(e. g., *Pedlosky*, 1998)

where ρ_0 and β are the average density of the water column and the meridional gradient of f respectively. Note that I converted mass to volume transport using a constant average density ρ_0 of 1025 kg m^{-3}. Finally, I computed ψ by integrating $V_{geos.}$, $M^y_{sv.}$, $M^y_{ek.}$ and $M^y_{geos.}$ across the basin (Equation 3).

$$\psi \equiv \int_x^{X_e} V dx, \tag{3}$$

where V can be the meridional velocity or transport, and X_e is the eastern boundary of the basin. In order constrain the circulation in the South Atlantic (i. e., close the basin), I imposed $V = 0$ over the African continent and at 20°E (i. e., where the Atlantic connects with the Indian ocean).

3 Results and Discussion

3.1 Geostrophic Estimates

The climatological ARGO-derived geostrophic stream function ($\psi_{geos.}$) estimates are shown in Figure 2. Note that in the upper 800 m of the water column, the subtropical circulation is dominated by a triangular-shaped anticyclonic gyre (i. e., the South Atlantic Subtropical Gyre) that extends from approximately 10°S to 40°S. As we go deeper in the water column, this gyre circulation becomes narrower (i. e., smaller meridional extension) and its maximum $\psi_{geos.}$ values at the western part of the domain (X_w) "migrate" southward. Additionally, the subtropical gyre seems to have some seasonal variability that is not clear and uniform at all depths.

In a first order, this circulation pattern (i. e., narrowing and "position" of the gyre) can be explained in the scope of the Ventilated Thermocline theory proposed by *Lyuten et al.* (1983). Although this theory was originally elaborated to explain the vertical structure of the tropical and subtropical thermocline, it also can be thought as a wind-driven large-scale circulation theory for a stratified ocean at mid- and low-latitudes. Specifically, the narrowing of the gyre is consistent with the growing area of the so-called **Shadow Zones** with depth [for details see *Pedlosky* (1998)]. Both narrowing and migration of the gyre "position" result from the geometry of the problem (i. e., boundary conditions, active layers characteristics, shape of the basin, wind forcing) and the conservation of potential vorticity (PV) along the streamlines[1].

At 2000 m depth (Figure 2 right panels), the gyre circulation is no longer observable and the flow is driven by the buoyancy forcing (i. e., thermohaline circulation signal). In order to visualize to what depth the gyre circulation extends in average, I computed the annual mean of the stream function [$\bar{\psi}(x,y,z)_{geos.}$] and plotted the $\bar{\psi}(x=X_w)_{geos.}$ at different latitudes (see Figure 3). As predicted by the Ventilated Thermocline theory, the shallower and thinner thermocline (or the active layers in the theory) reflects the fact that the wind-driven circulation decays "faster" at lower latitudes [i. e., $\bar{\psi}(x=X_w)_{geos.}=0$ are located at lower depths at lower latitudes]. Figure 3 shows that $\bar{\psi}(x=X_w)_{geos.}=0$ is placed at approximately 500 m (1400 m) at 15.5°S (30.5°S).

[1] PV balance is Sverdrupian ($\beta v = f\frac{\partial w}{\partial z}$) off the western boundary layer

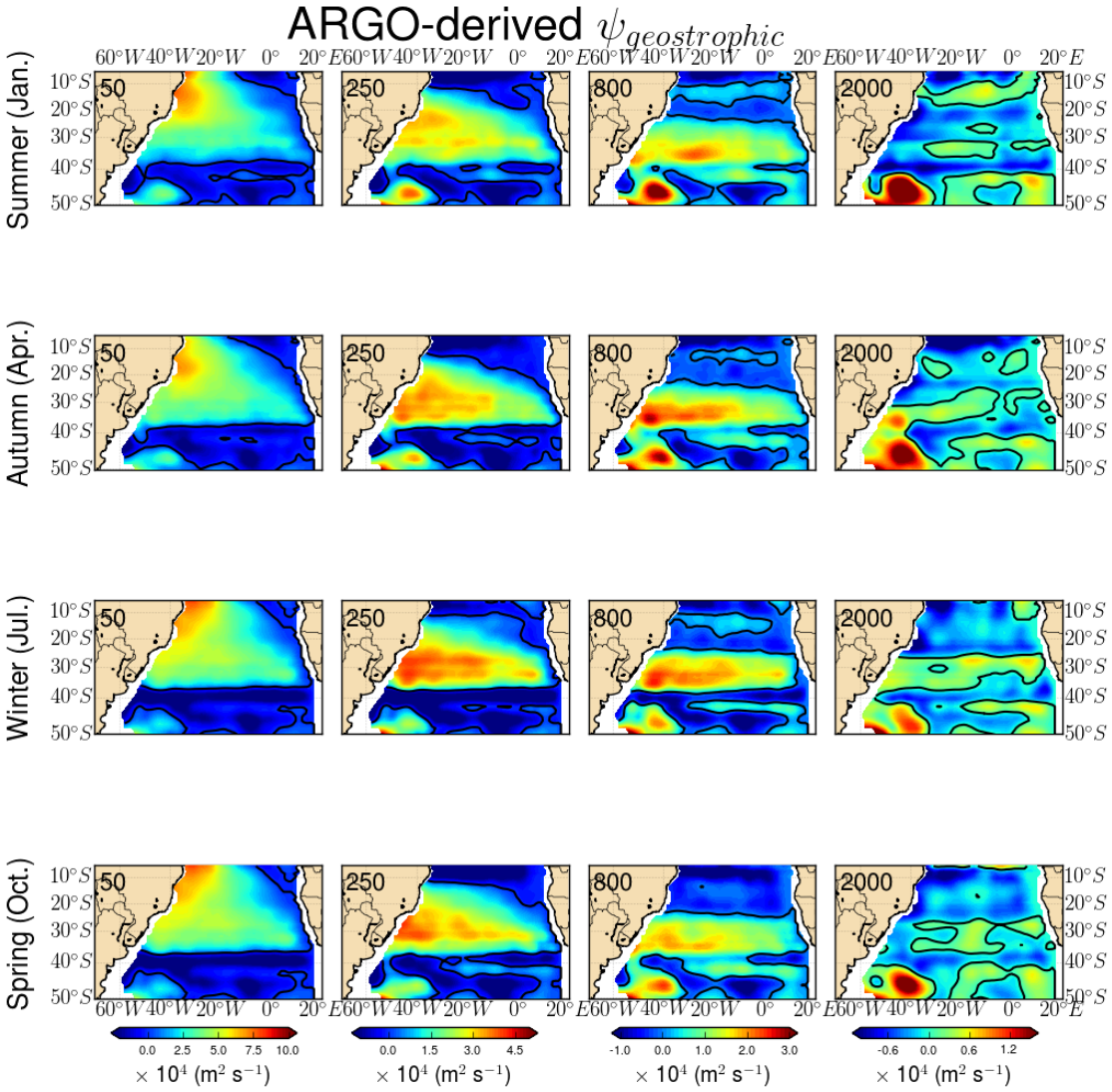

Figure 2: ARGO-derived geostrophic stream function at depths 50, 250, 800 and 2000 m (columns of panels) and austral season (rows of panels). Note that the color scales are different at each depth, in order to highlight the stream function gradients.

Note that the profile at 40.5°S (magenta line) is not within the subtropical gyre, additionally the profile at 35.5°S is close to the southern limit of the gyre (i. e., Brazil-Malvinas Confluence) therefore it is not possible to estimate the vertical extension of the wind-driven circulation at those latitudes. Therefore, based on the $\bar{\psi}(x = X_w)_{geos.}$ profiles at mid-latitudes I assumed a vertical of approximately 1200 m of the wind-driven circulation signal, which is consistent with the depth of the base of the thermocline in the open ocean (e. g., *Talley et al.*, 2011).

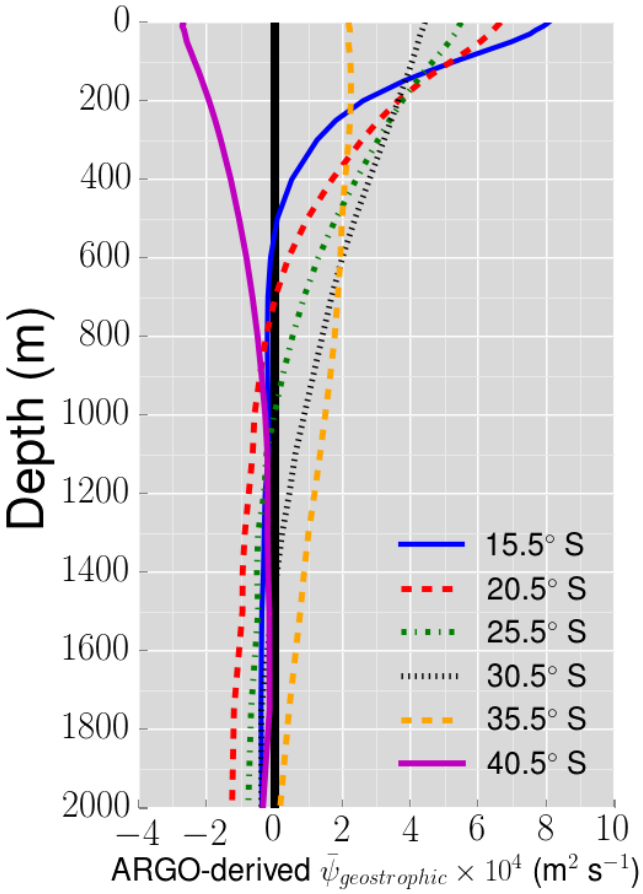

Figure 3: Annual mean of the ARGO-derived geostrophic stream function ($\bar{\psi}_{geos.}$) profiles at the western grid data point (X_w).

3.2 Sverdrup and Ekman theories

Combining the results of Sverdrup and Ekman transports (e. g., Equation 2), I computed the wind-derived vertically integrated geostrophic stream function ($\psi_{Sv.} - \psi_{Ek.}$) and presented it in Figure 4. This steady state solution for the vertically integrated circulation presents a seasonal variability consistent with the wind-stress curl distributions and meridional displacement of the atmospheric synoptic-scale wind patterns over the South Atlantic. In other words, the southward displacement of the oceanic gyre is related to the respective migration of the wind pattern (e. g., *Risien and Chelton*, 2008).

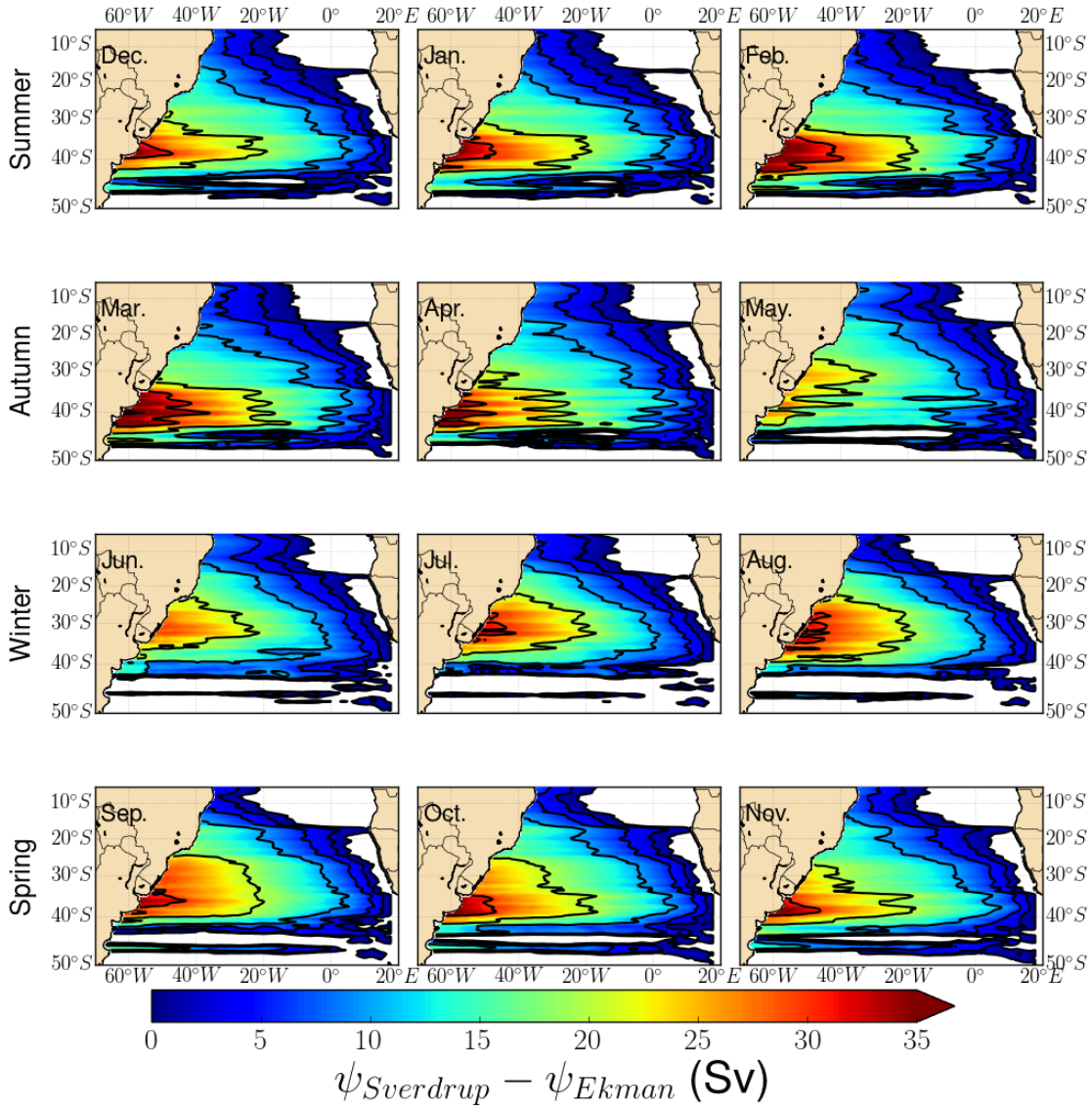

Figure 4: Vertically integrated wind-derived geostrophic stream function over the water column. Each row of panels indicate one austral season. The black contours indicate the streamlines of 0, 2, 5, 10, 20, 30, and 40 Sv.

3.3 ARGO vs Sverdrup

In order make both applied methods comparable, I integrated the ARGO-derived $\psi_{geos.}$ over the upper 1200 m (i. e., approximate extension of the wind-driven circulation). Although the seasonal variability presented in Figures 2 and 4 are evident and distinct, the analysis of the circulation features and magnitude of the Western Boundary Current volume transport were performed using its annual mean for simplicity.

The upper panels from Figure 5 depict the vertically integrated geostrophic circulation patterns. Clearly,

both patterns are different in dimension, intensity, and present different dominant features south of ∼40°S. In terms of non-Sverdrupian dynamics (see right upper panel from Figure 5), it is possible to notice two prominent features at the southwest corner of the domain: the Zapiola Eddy, and a northward current that seems to be part of the Malvinas Current (MC). The first is a large anticyclonic eddy generated by flow-topography interactions between the eastward Antartic Circumpolar Current (ACC) and a sea-mount called the Zapiola Rise, and the later is a branch of the ACC that flows along the South American continental slope. In fact, the collision between the MC and the Western Boundary Current (i. e., the Brazil Current or BC) forces both currents to turn offshore and separate from the coast at approximately 40°S (e. g., *S Imawaki et al.*, 2013; *Talley et al.*, 2011). Note the Sverdrup theory (left upper panel from Figure 5) predicts the BC separation from the coast at approximately 45°S, which might explain the large differences in the cross-basin integrated meridional transports close to the confluence.

If we continue comparing the structural differences of the gyres, an ambiguous interpretation can arise. The Figure 5 (lower panel) shows that the zonally integrated ARGO-derived geostrophic transport agrees well with the wind-derived between approximately 10°- 35°S. This unexpected agreement could indicate that the Sverdrupian dynamics exclusively forced by the wind dominates the PV balance, however the evident differences in the interior streamlines suggest something else. Note that the line of 20 Sv in the ARGO-derived gyre is much closer to the basin eastern boundary than in the wind-derived gyre indicating a more strong flow. We can speculate that this feature could be associated with changes in the PV balance in that region and the Agulhas Leakage [i. e., transport of water from the Idian Ocean to the Atlantic, see *S Imawaki et al.* (2013)].

In terms of the BC volume transport [i. e., compensatory transport that has opposite sign of $\bar{\psi}(x = X_w)_{sv.}$[2]] it is difficult to discuss climatological patterns due to the lack of long term monitoring of the BC transport, however it is known from scattered synoptic observations, and estimates combining ARGO floats and altimetric data that its transport increases from approximately 3-6 to 25 Sv between 22 and 35°S (e.g., *Schmid*, 2014).

We know that it is expected to observe a BC transport much lower than the values of $\bar{\psi}(x = X_w)_{geos.}$ due to the presence of the buoyancy-driven circulation transport upper branch (a.k.a. MOC[3] transport)

[2]Wind-driven western boundary layer transport is $\bar{\psi}(x = X_w)_{sv.} = \bar{\psi}(x = X_w)_{geos.} + \bar{\psi}(x = X_w)_{ek.}$

[3]MOC: Meridional Overturning Circulation (e.g., *S Imawaki et al.*, 2013)

following the interior "Sverdrupian" streamlines. This concept was introduced by *Stommel* (1965), and it was used to explain why the BC volume transport is lower than the Gulf Stream.

Almost two decades later, observations have shown that the BC flows over an intermediate counter-current (500-1200 depth) called Intermediate Western Boundary Current (IW) between ∼10-30°S. This counter-current is not predicted by *Stommel* (1965)'s argument (e.g., *Evans and Signorini*, 1985; *Boebel et al.*, 1999; *Legeais et al.*, 2013), therefore we should expect that part of MOC has to flow within the western boundary layer at latitudes lower then 30°S. In this sense, we can argue if the upper MOC branch transport uses the interior streamlines, it must be confined at depths around 700-1200 m, where the Subtropical Gyres recirculates at higher latitudes (e. g., Figure 2).

As an example of how the BC transport would be affected, lets consider the latitude of 25°S. At this latitude the ARGO-derived $\bar{\psi}(x = X_w)_{geos.}$ is ∼20 Sv, additionally the $\bar{\psi}(x = X_w)_{ek.}$ from Ekman theory is approximately -3 Sv, therefore the Sverdrup transport will be 17 Sv at 25°S. Recent and historical synoptic observations have shown the BC is transporting -3 to -7 Sv over the continental slope between 23-25°S above the IWBC (*Silveira et al.*, 2004; *Rocha et al.*, 2014; *Biló et al.*, 2014; *Schmid*, 2014). Assuming the mean climatological BC transports approximately -5 Sv (purely arbitrary choice) and the presence of this intermediate current, the MOC should be transporting at least ∼12 Sv (i. e., MOC = -5 + 17) in the boundary layer. Considering the MOC transports 15 Sv northward, the other 3 Sv will use the upper streamlines of the gyre (i. e., approximately 0-700 m).

It is important to keep in mind that these estimates must be carefully interpreted due to the high uncertainties involved in the ARGO-derived estimates, applied boundary conditions, and not rigorous assessment of the Subtropical Gyre vertical extension. Therefore, these results only suggests such MOC pathway.

4 Conclusions

To conclude, I summarized the results answering the questions presented in Section 1.

1. **How does the geostrophic circulation change with depth?** As we go deeper in the water column, the geostrophic Subtropical Gyre becomes less intense, narrower (i. e., its northern limit migrates southward), and its center migrates southward.

2. **To what depth does the gyre circulation extend, and how does this vary with location within the gyre?** Its extends to approximately 1200 m. As we move to higher latitudes the vertical extension of the gyre increases (i. e., ocean becomes more barotropic).

3. **To what degree is the circulation consistent with Sverdrup theory, and how do the results compare to what is known about the transport of the respective western boundary currents?** Although there are some important structural differences in the Subtropical Gyre, the Svredrup theory represents well the mean horizontally and vertically integrated geostrophic transport between 10-35°S.

   Additionally, I speculated that most of the MOC upper branch (or warm) pathway in the South Atlantic should be confined in the western boundary layer and how this generates a much weaker BC than expected from Sverdrup Theory. In terms of seasonal variability, the Sverdrup theory does not explain the geostrophic variations due to the adjustment time of the total flow to changes in the wind-forcing mechanisms (see Figure 8 in the appendix for a more clear picture).

4. **Are there any interesting features that may be associated with non-Sverdrupian dynamics, and what are they related to?** Yes. The most obvious one is the Zapiola Eddy placed on the southwestern part of the Basin. It is generated by the interaction between a sea-mount and the ACC eastward flow.

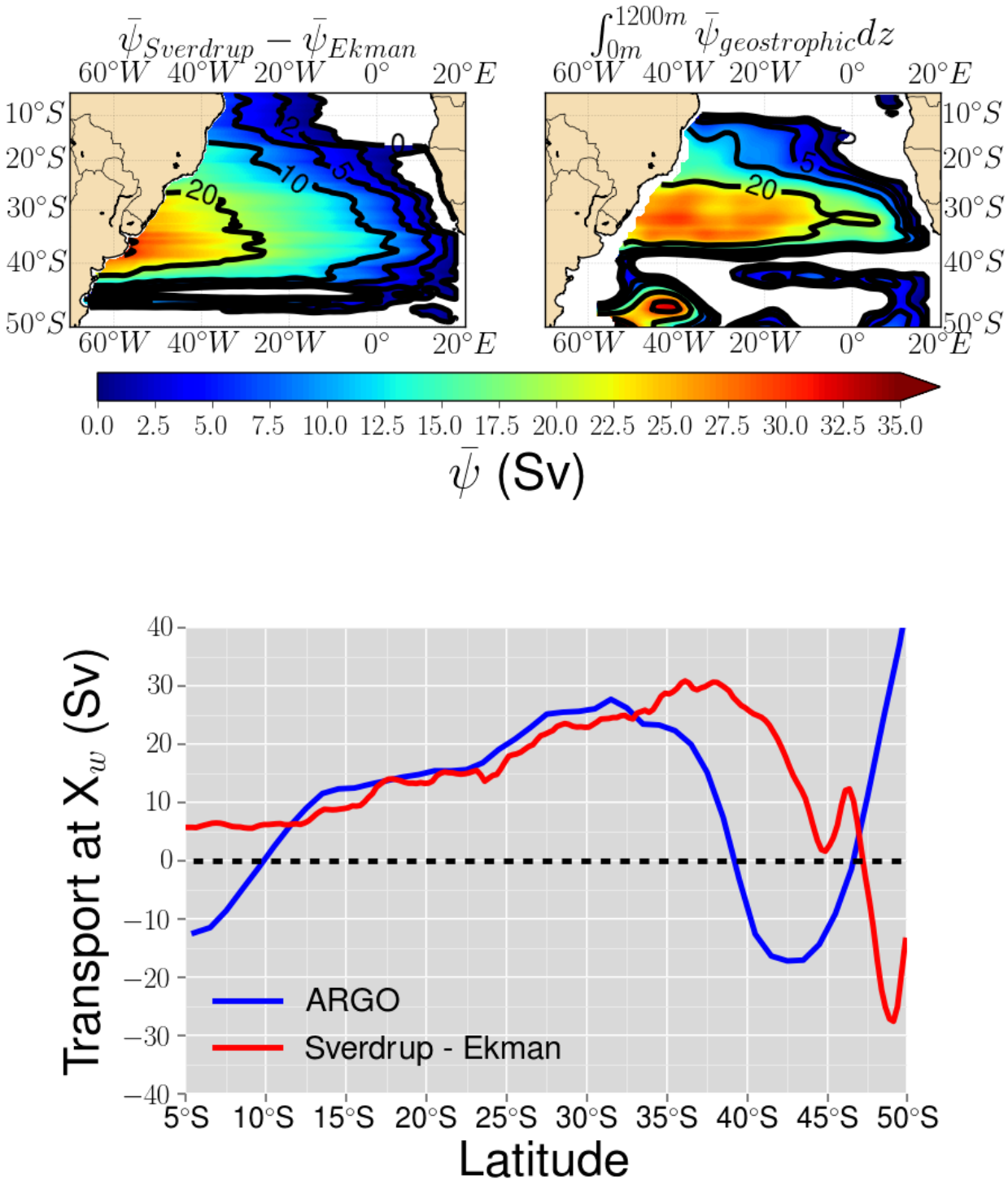

Figure 5: Annual mean of the vertically integrated geostrophic stream function ($\bar{\psi}$) derived from ARGO and wind data (upper panels). $\bar{\psi}(x = X_w)$ values (or x- and z-integrated transport) at different latitudes (lower panel).

References

Biló, T. C., I. C. A. da Silveira, W. C. Belo, B. M. Castro, and A. R. Piola (2014), Methods for estimating the velocities of the Brazil Current in the pre-salt reservoir area off southeast Brazil, *64*, 1431–1446.

Boebel, O., R. E. Davis, M. Ollitrault, R. G. Peterson, P. L. Richardson, C. Schmid, and W. Zenk (1999), The Intermediate Depth Circulation of the Western South Atlantic, *Geophys. Res. Lett.*, *26*(21), 3329–3332.

Evans, D. L., and S. R. Signorini (1985), Vertical structure of the Brazill Current, *Nature*, *315*, 48–50.

Legeais, J.-F., M. Ollitrault, and M. Arhan (2013), Lagrangian observations in the Intermediate Western Boundary Current of the South Atlantic, *85*, 109–126.

Lyuten, J. R., J. Pedlosky, and H. Stommel (1983), The Ventilated Thermocline, *J. Phys. Oceanogr.*, *13*, 292–309.

Pedlosky, J. (1998), *Ocean Circulation Theory*, first ed., Springer, NY.

Rio, M. H. S., S. Guinehut, and G. Larnicol (2011), New CNES-CLS09 global mean dynamic topography computed from the combination of GRACE data, altimetry, and in situ measurements, *116*(C07018), doi:10.1029/2010JC006505.

Risien, C. M., and D. B. Chelton (2008), A Global Climatology of Surface Wind and Wind Stress Fields from Eight Years of QuickSCAT Scatterometer Data, *J. Phys. Oceanogr.*, *38*, 2379–2413.

Rocha, C. B., I. C. A. da Silveira, B. M. Castro, and J. A. M. Lima (2014), Vertical structure, energetics and dynamics of the Brazil Current System at 22°S-28°S, doi:10.1002/2013JC009143.

S Imawaki, A. S. B., L. Beal, and B. Qiu (2013), *Ocean Circulation and Climate - a 21 st century perspective*, chap. Western Boundary Currents, 2ªed., Academic Press, London.

Schmid, C. (2014), Mean vertical and horizontal structure of the subtropical circulation in the South Atlantic from three-dimensional observed velocity fields, *Deep Sea Research Part I: Oceanographic Research Papers*, *91*, 50–71.

Silveira, I. C. A., L. Calado, B. M. de Castro, M. Cirano, J. A. M. Lima, and A. S. Mascarenhas (2004), On the Baroclinic Structure of the Brazil Current-Intermediate Western Boundary Current at 22°-23°S, *Geophys. Res. Lett.*, *31*, 4308.

Stommel, H. (1965), *The Gulf Stream: A Physical and Dynamical Description*, University of California Press.

Talley, L. D., G. L. Pickard, W. J. Emery, and J. H. Swift (2011), *Descriptive Physical Oceanography: An Introduction*, sixth ed., Academic Press.

Appendix

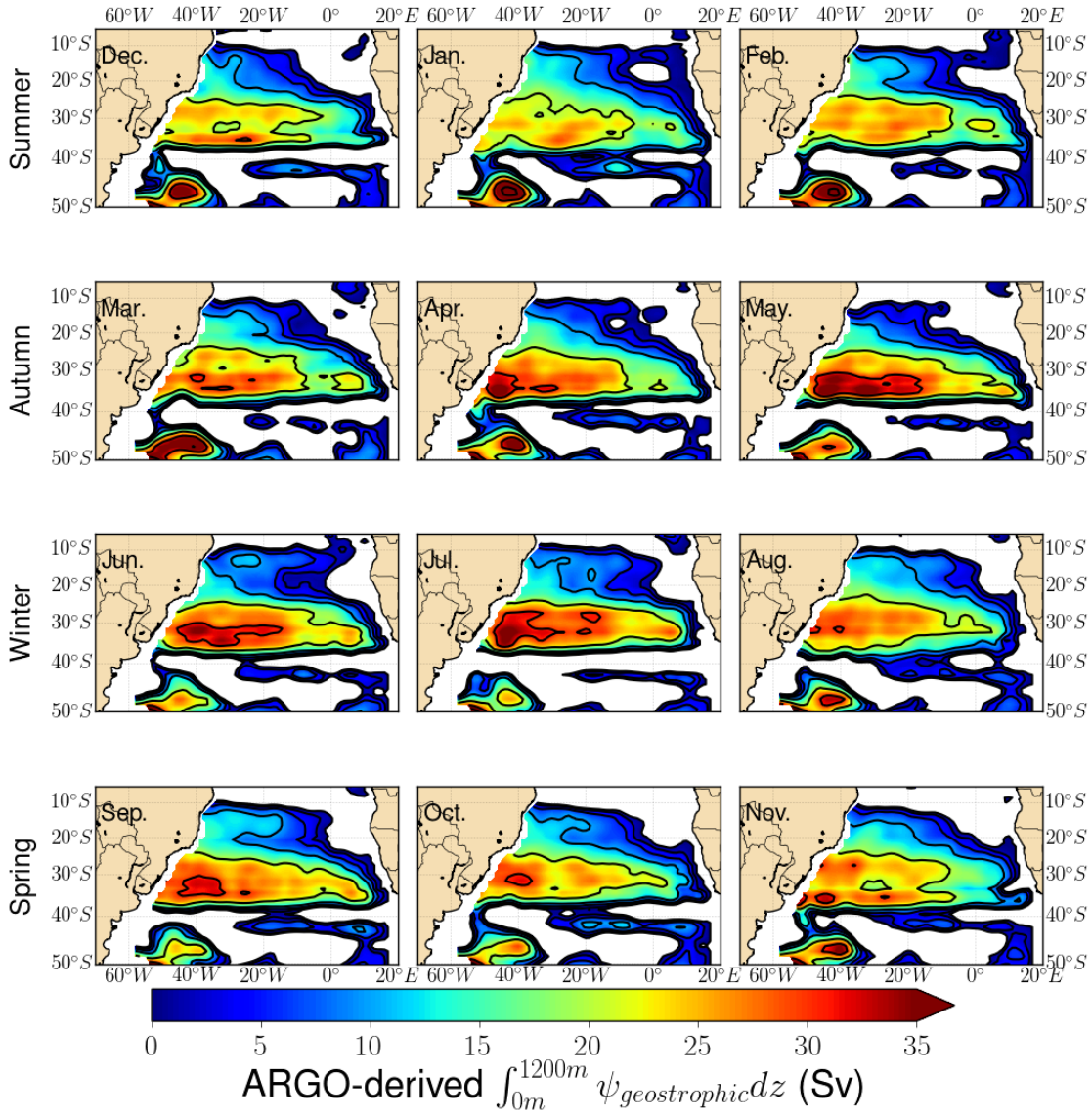

Figure 6: Vertically integrated ARGO-derived geostrophic stream function between surface and 1200 m depth. Each row of panels indicate one austral season. The black contours indicate the streamlines of 0, 2, 5, 10, 20, 30, and 40 Sv.

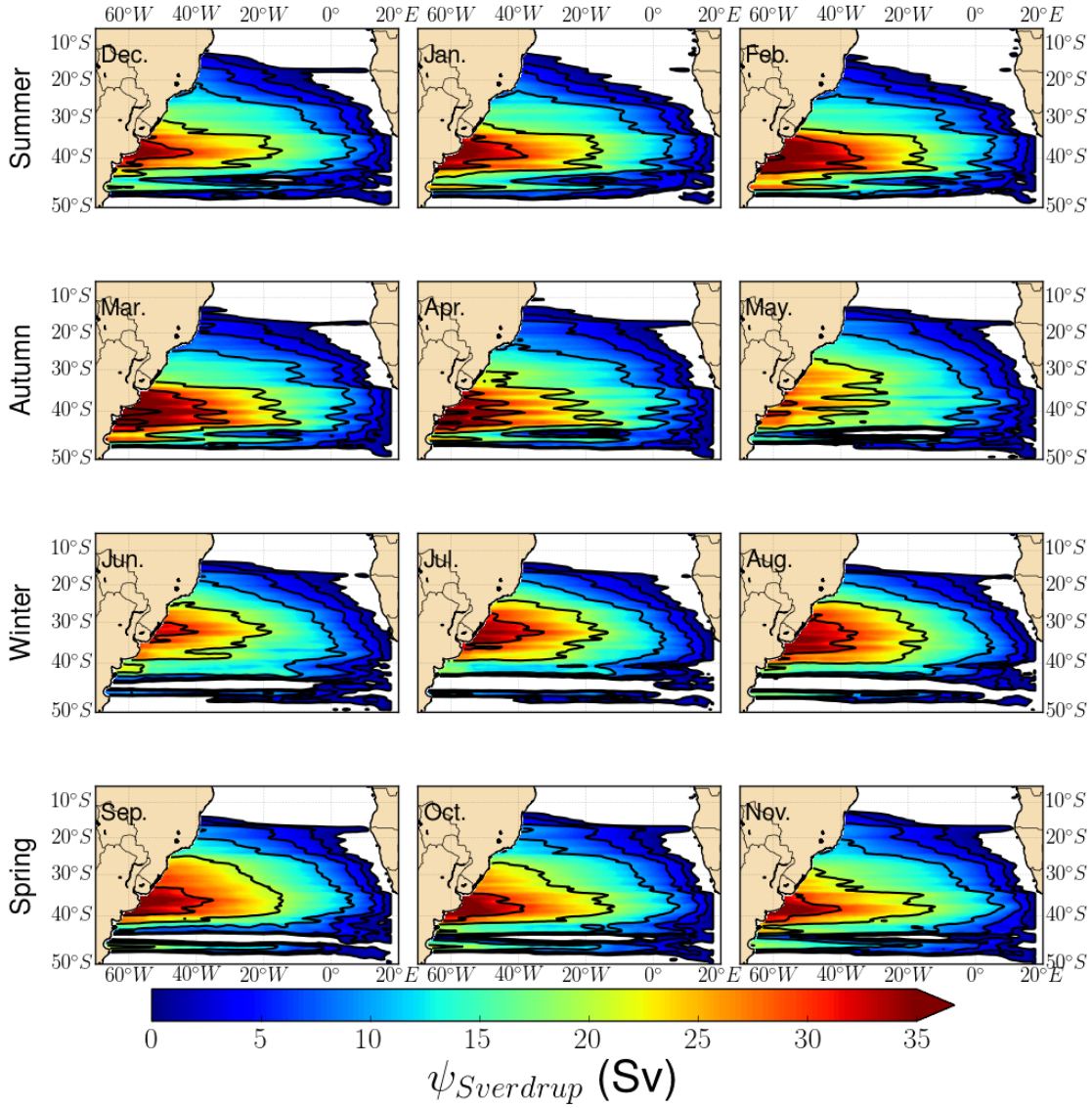

Figure 7: Sverdrup stream function over the water column. Each row of panels indicate one austral season. The black contours indicate the streamlines of 0, 2, 5, 10, 20, 30, and 40 Sv.

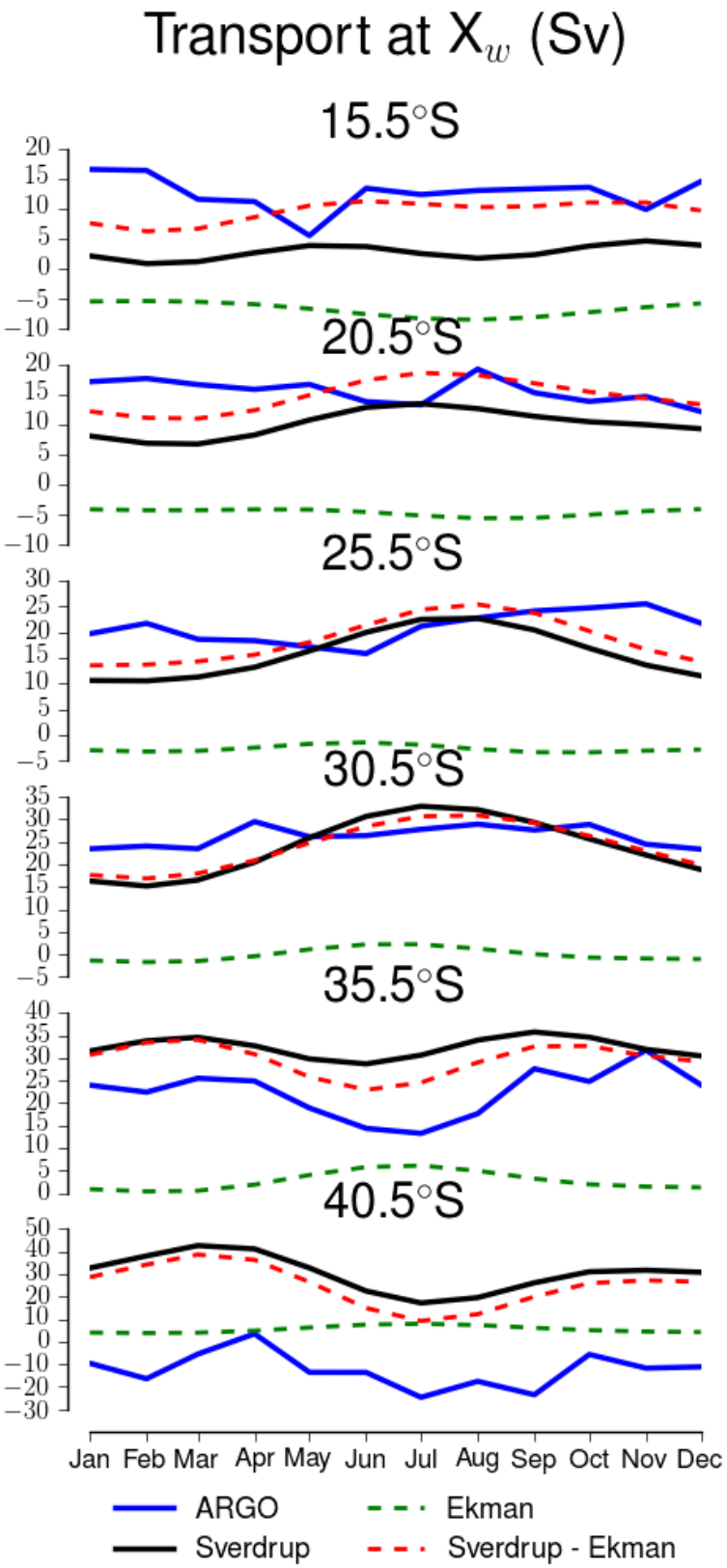

Figure 8: Monthly $\psi(x = X_w)$ values (or x- and z-integrated transport) at different latitudes.